Supplemental Material for "Elliott-Yafet Spin-Phonon Relaxation Times from First Principles"

Jinsoo Park,[1] Jin-Jian Zhou,[1] and Marco Bernardi[1,*]

[1]*Department of Applied Physics and Materials Science, California Institute of Technology, Pasadena, California 91125, USA*

Importance sampling approach for computing spin-flip relaxation times

Figure S1 compares the convergence of $\tau_{n\boldsymbol{k}}^{\text{flip}}$ with a random sampling approach and with our importance sampling method. The convergence rate of the importance sampling approach is orders of magnitude faster than random sampling. For example, the required number of $\boldsymbol{q}$-points to reach a 1% error for the importance sampling method is $30,000$, versus a much larger value of 65 million points for the random sampling method. The considerable time saving afforded by our importance sampling method allows us to fully converge the spin relaxation times.

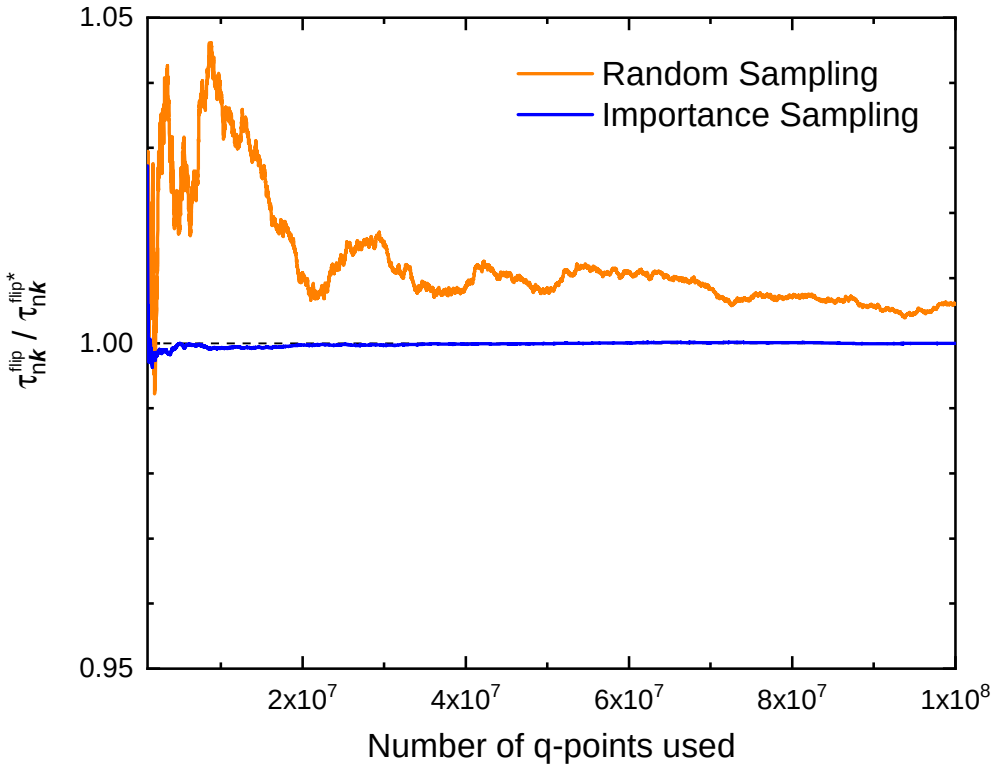

FIG. S1. Comparison between the convergence of the random sampling method (orange line) and the importance sampling method (blue line). The initial electron band n and momentum $\boldsymbol{k}$ are set to the conduction band minimum, and only the f process is considered to illustrate the convergence trend. Shown is the ratio between the computed $\tau_{n\boldsymbol{k}}^{\text{flip}}$ and the converged value $\tau_{n\boldsymbol{k}}^{\text{flip}*}$, which is computed with a $1000 \times 1000 \times 1000$ $\boldsymbol{q}$-point BZ grid. The $P_{\boldsymbol{k}}(\boldsymbol{q})$ distribution used in the importance sampling method is computed using a $100 \times 100 \times 100$ $\boldsymbol{q}$-point grid.

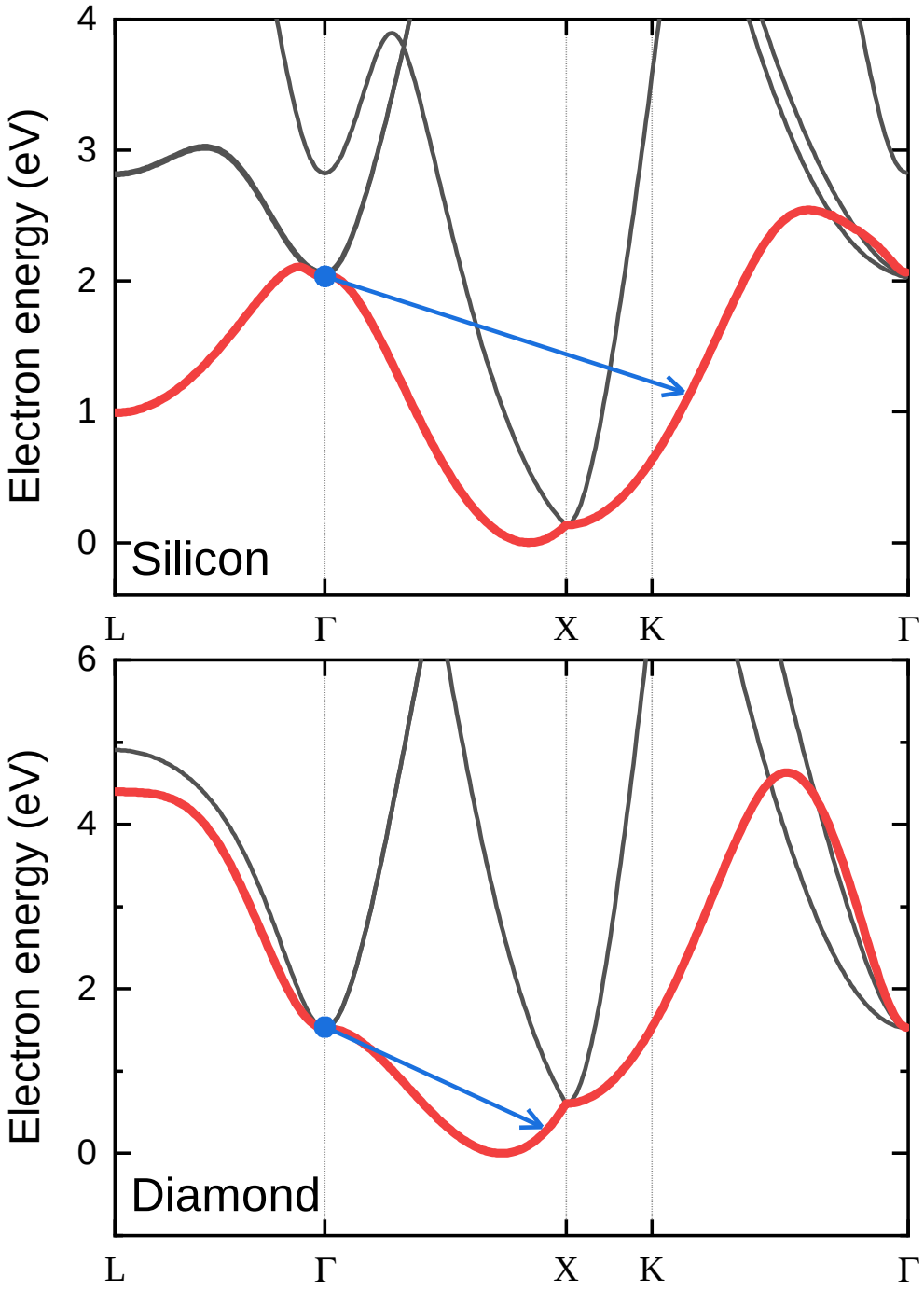

FIG. S2. The low-energy spin-degenerate conduction band in silicon and diamond chosen to compute the ratio between the spin-flip and the momentum-scattering e-ph matrix elements in Fig. 2 of the main text. The blue circle is the initial electronic state.

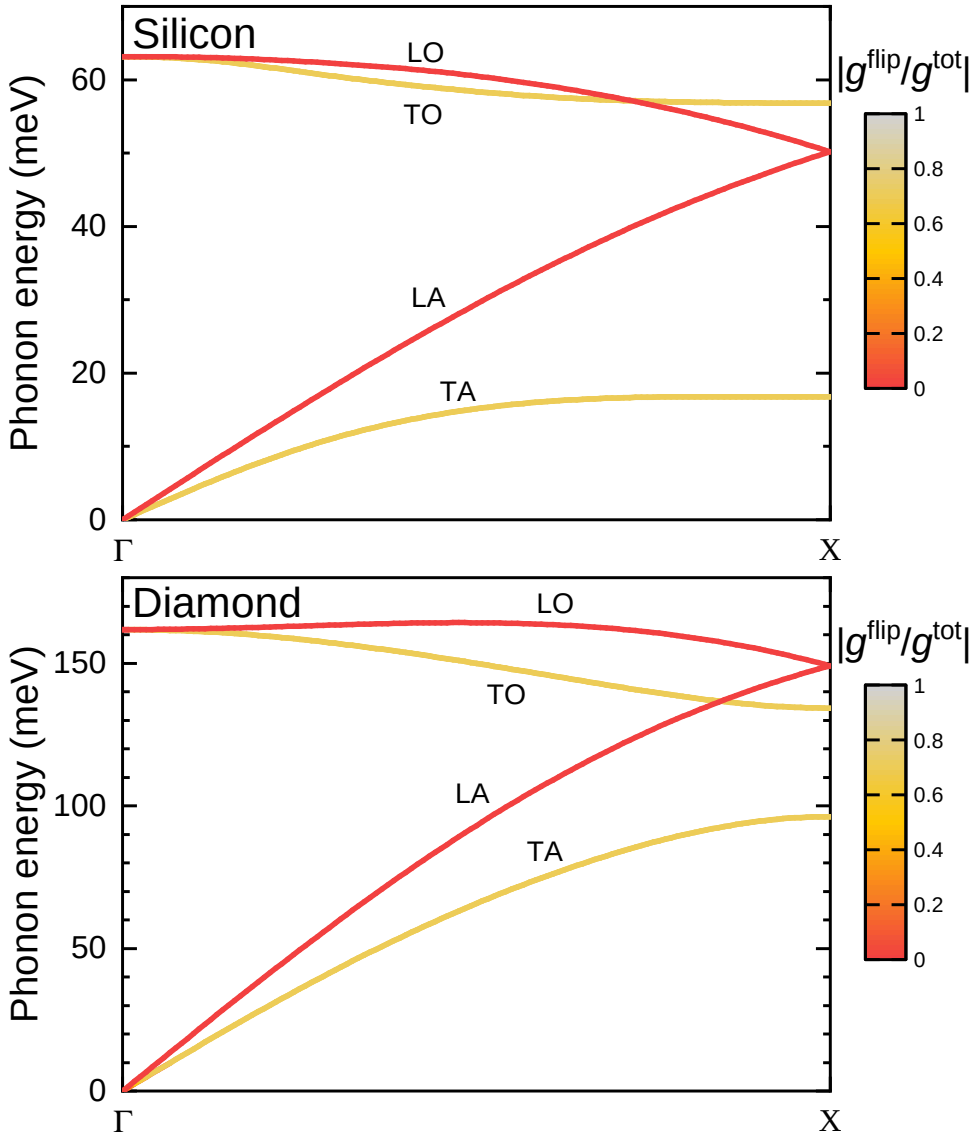

FIG. S3. Phonon dispersions in silicon and diamond, overlaid with a color map of the ratio $\left|g_\nu^{\text{flip}}(\boldsymbol{q})/g_\nu^{\text{tot}}(\boldsymbol{q})\right|$ between the spin-flip and the total (i.e. momentum-scattering) e-ph matrix elements; the two matrix elements differ by orders of magnitude for the branches shown in red. The data shown are the square root of the gauge-invariant trace of $|g|^2$ over a low-energy spin-degenerate conduction band shown in Fig. S2. The initial electron momentum is set to the X point, which is different from the Γ point used in Fig. 2 of the main text, and we plot the ratio for phonon wave vectors $\boldsymbol{q}$ along Γ−X.

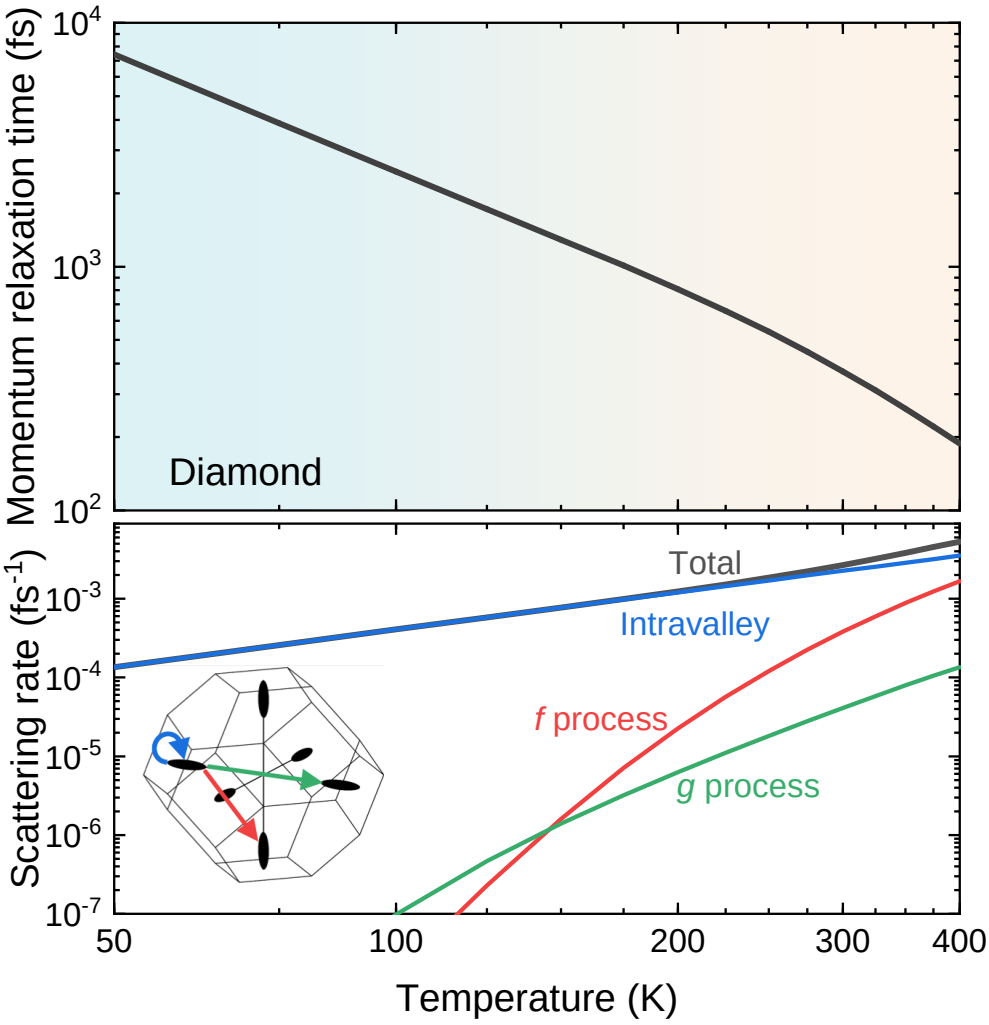

FIG. S4. Computed momentum relaxation times as a function of temperature in diamond. The lower panel shows the process-resolved momentum-scattering e-ph scattering rates, defined as the inverse of the momentum relaxation time τ_p (see the main text). Shown are the contributions from intravalley processes (blue line), f processes (red line) and g processes (green line), which add up to the total (gray line). It is seen that for momentum scattering in diamond, intravalley scattering dominates over the entire temperature range, while for spin relaxation the intravalley processes are dominant only below 170 K (see the main text).

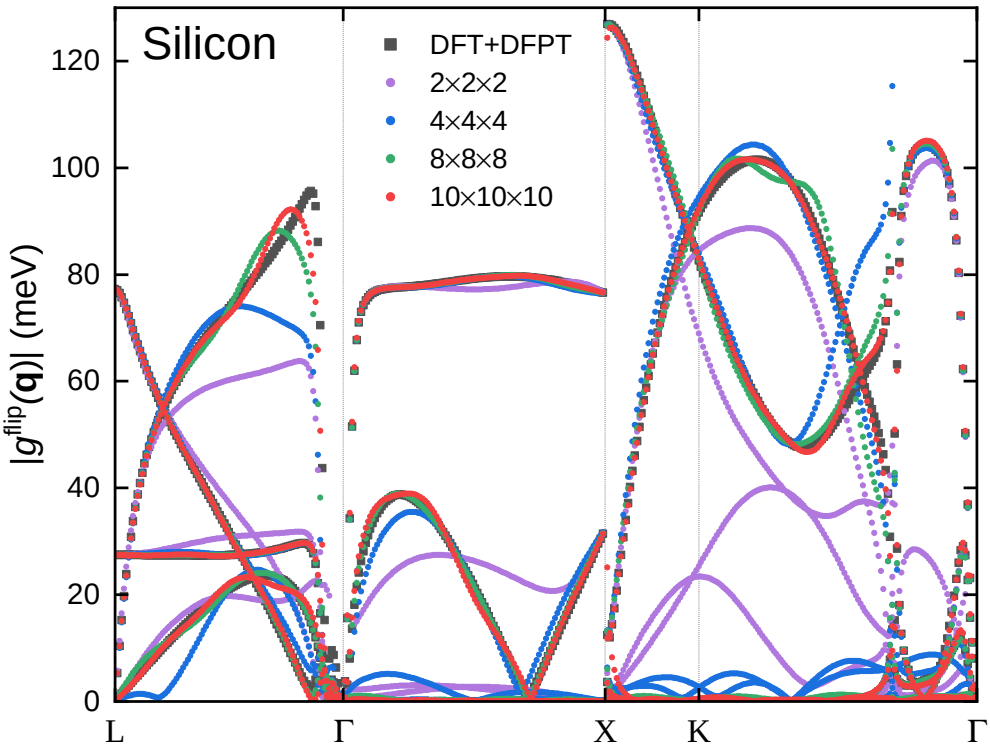

FIG. S5. Comparison between the spin-flip e-ph matrix elements $\left|g_\nu^{\rm flip}(\boldsymbol{q})\right|$ computed with DFPT (gray squares) and those obtained from our Wannier interpolation scheme discussed in the main text. For the latter, we show results obtained with coarse $\boldsymbol{q}$-point grids of $2\times2\times2$ (purple dots), $4\times4\times4$ (blue dots), $8\times8\times8$ (green dots) and $10\times10\times10$ (red dots). It is seen that $8\times8\times8$ or finer $\boldsymbol{q}$-point grids, as we used in our work, are sufficient for accurately interpolating the DFPT e-ph matrix elements. The data shown are for silicon, and we plot the square root of the gauge-invariant trace of $|g|^2$ over the lowest spin-degenerate conduction band. The initial electron momentum is set to the Γ point and we plot the matrix elements for phonon wave vectors $\boldsymbol{q}$ along a high-symmetry BZ line.

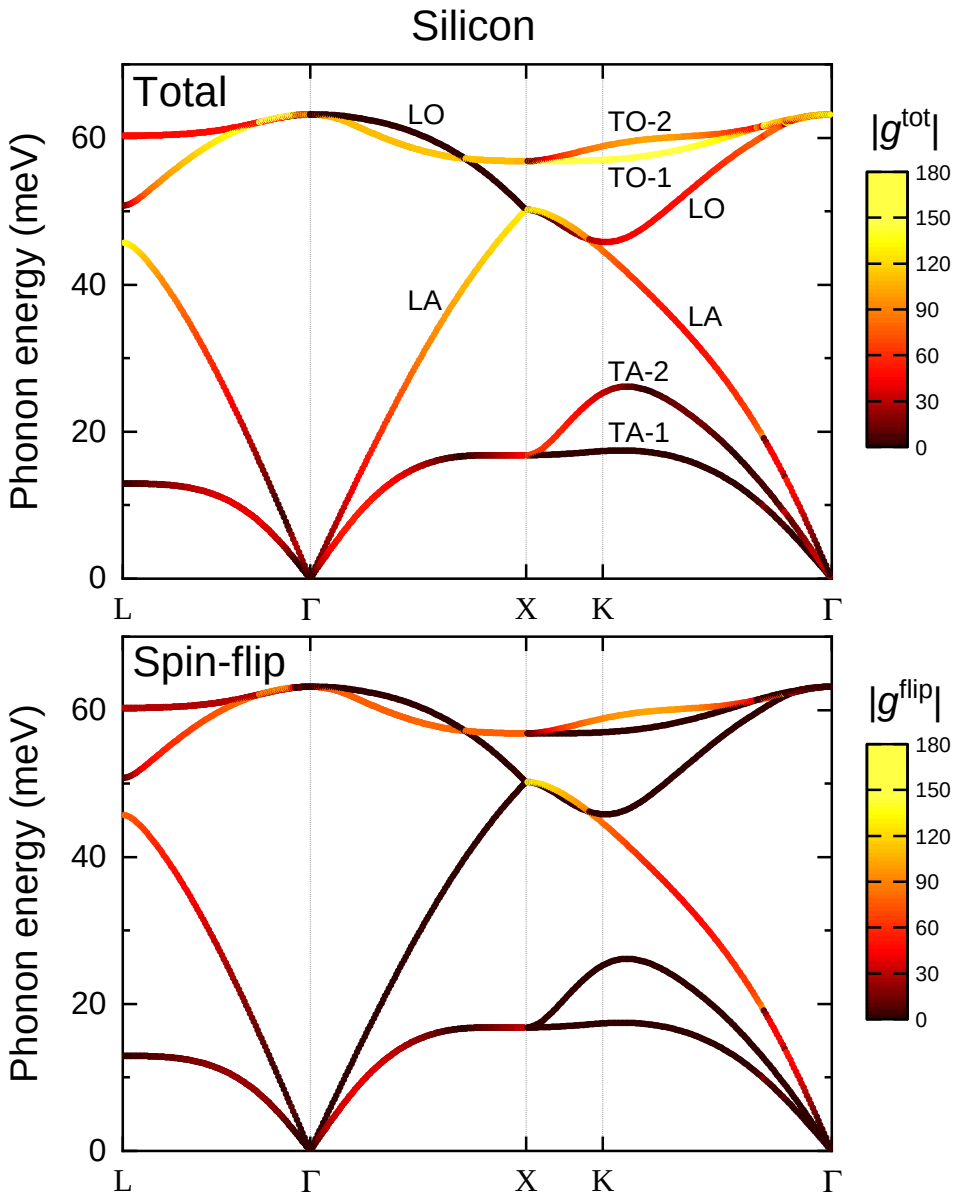

FIG. S6. Phonon dispersions in silicon, overlaid with a color map of the total (i.e. momentum-scattering) e-ph matrix elements $\left|g_\nu^{\text{flip}}(\boldsymbol{q})\right|$ (upper panel) and the spin-flip e-ph matrix elements $\left|g_\nu^{\text{tot}}(\boldsymbol{q})\right|$ (lower panel). The data shown are the square root of the gauge-invariant trace of $|g|^2$ for a low-energy spin-degenerate conduction band (see Fig. S2). The initial electron momentum is set to the Γ point and we plot the values for phonon wave vectors $\boldsymbol{q}$ along a high-symmetry BZ line.

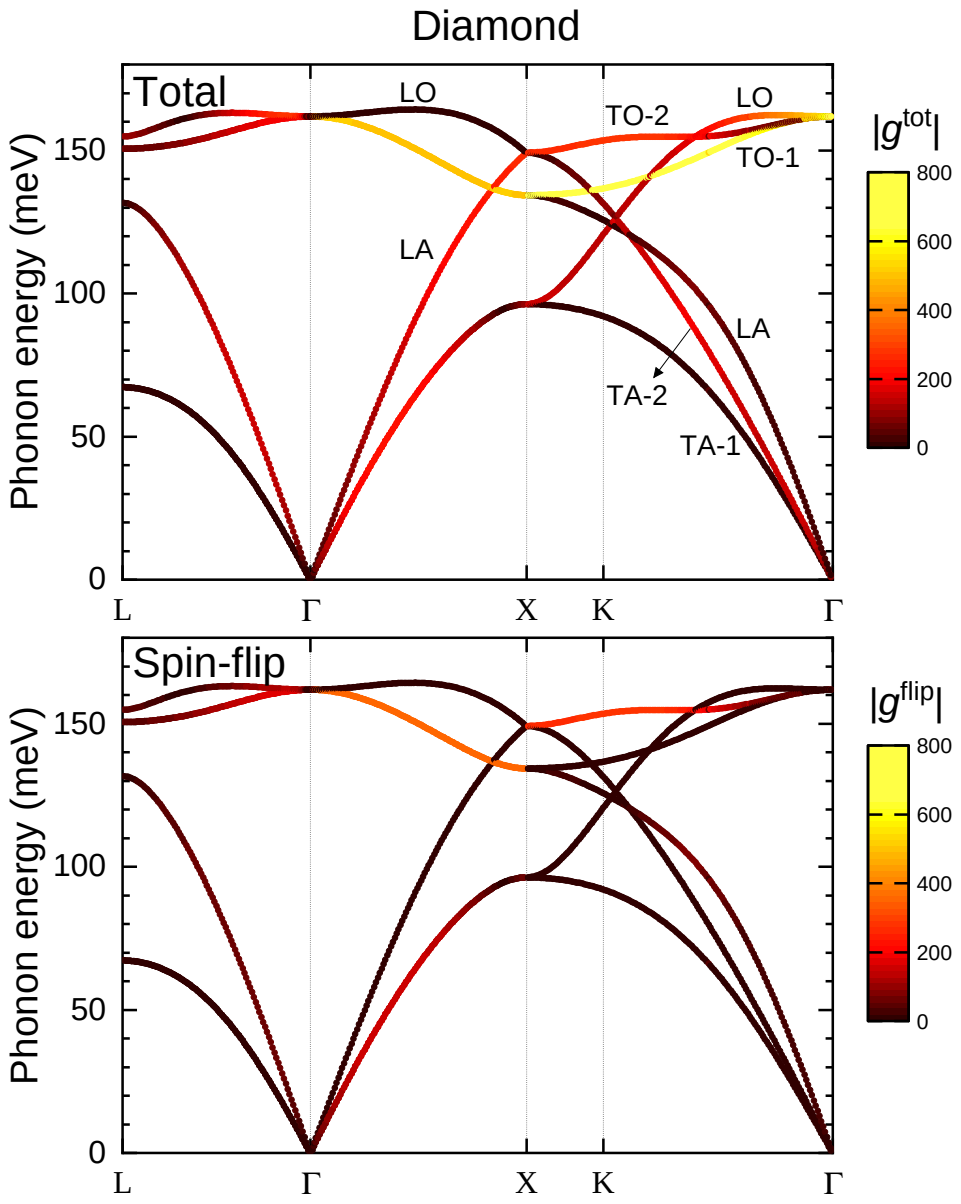

FIG. S7. Phonon dispersions in diamond, overlaid with a color map of the total (i.e. momentum-scattering) e-ph matrix elements $\left|g_\nu^{\text{flip}}(\boldsymbol{q})\right|$ (upper panel) and the spin-flip e-ph matrix elements $\left|g_\nu^{\text{tot}}(\boldsymbol{q})\right|$ (lower panel). The data shown are the square root of the gauge-invariant trace of $|g|^2$ for a low-energy spin-degenerate conduction band (see Fig. S2). The initial electron momentum is set to the Γ point and we plot the values for phonon wave vectors $\boldsymbol{q}$ along a high-symmetry BZ line.

* bmarco@caltech.edu

[1] J.-J. Zhou and M. Bernardi, Phys. Rev. B **94**, 201201 (2016).